Journal of Solid State Chemistry 241 (2016) 137–142

Contents lists available at ScienceDirect

Journal of Solid State Chemistry

journal homepage: www.elsevier.com/locate/jssc

Effective reduction in the nanoparticle sizes of NiO obtained via the pyrolysis of nickel malonate precursor modified using oleylamine surfactant

Roussin Lontio Fomekong [a,b,*], John Ngolui Lambi [a], Guy Roland Ebede [a], Patrice Kenfack Tsobnang [c], Hypolite Mathias Tedjieukeng Kamta [a], Cedrik Ngnintedem Yonti [a], Arnaud Delcorte [b]

[a] Chemistry Department, Higher Teacher Training College, University of Yaoundé I, B.P. 47, Yaoundé, Cameroon
[b] Institut de la Matière Condensée et des Nanosciences, Université Catholique de Louvain, Croix du Sud 1, 1348 Louvain-La-Neuve, Belgium
[c] Chemistry Department, University of Dschang, PO Box 96, Dschang, Cameroon

ARTICLE INFO

Article history:
Received 24 March 2016
Received in revised form
9 June 2016
Accepted 10 June 2016
Available online 14 June 2016

Keywords:
Nickel oxide
Nickel malonate
Precipitation
Oleylamine
Particle sizes

ABSTRACT

Nickel oxide nanoparticles were synthesized via thermal decomposition of two precursors, the first, a simple nickel malonate and the second, a nickel malonate modified by oleylamine, a surfactant, both having been synthesized by precipitation. While FTIR, TGA and ToF-SIMS were used to characterize the two precursors and to show the presence of oleylamine in the modified precursor, XRD, SEM, TEM and BET were employed to investigate the structure, the morphology and the specific surface area of the decomposition products obtained after pyrolysis. The results showed that the modification of nickel malonate by oleylamine was effective. The XRD results, which showed a cubic structure for the NiO obtained, suggest with SEM an important particle size reduction (at least 54%) when oleylamine was used to modify the nickel malonate precursor. The SEM images also showed a well-defined spherical nanoparticle morphology in both cases, not affected by the presence of oleylamine. The TEM also confirmed the reduction of particle size and their spherical nature but at the same time showed that, in the presence of oleylamine, there was no agglomeration resulting in a more uniform particle size distribution. The specific surface area of the NiO obtained by the oleylamine-modified precursor was 4.7 times larger than that obtained with the regular precursor. This again confirms the particle size reduction.

1. Introduction

Nanoscale materials display physical and chemical properties that are different from those of their bulk counterparts [1]. This difference can be attributed to surface effects (causing smooth properties scaling as a function of the fraction of atoms at the surface) and to quantum effects (showing discontinuous behavior due to quantum confinement effects in materials with delocalized electrons) [1]. In fact the particle size influences the physical phenomena occurring in the material (electron and heat transfer, for example). For instance, the surface area of a material increases with decreasing particle size, and this affects directly many properties such as catalysis and gas sensing [2,3]. As a result, a new range of technological applications of nanomaterials has been developed in the last decade. For these reasons, design and optimization of synthetic methods for the production of nanoparticles have been intensively investigated and important progress has been made in the synthesis of nanomaterials with tailored composition, size, shape, and crystalline structure. However, there is still a strong need for the development of simple and inexpensive protocols for large-scale synthesis of high quality nanoparticles.

Nickel oxide (NiO) nanoparticles have particularly attracted the attention of scientists because of their very interesting characteristics such as good chemical stability, good optical, magnetic and electrical properties, and the fact that they are frequently used as a model for p-type metal oxide materials [4–6]. The electronic properties of NiO have specifically driven research interests in applications such as anodes for lithium ion batteries [7], solar cells [8], electrochromic coatings [9], composite anodes for fuel cells [10], antiferromagnetic materials [11] and gas sensors [12,13]. Regarding its synthesis, several methods have been reported in the literature, notably, solvo/hydrothermal reaction [14], sol–gel process [15], microwave synthesis [16], solution–combustion [17] and

* Corresponding author.
E-mail addresses: lonforou@yahoo.fr, roussin.lontio@uclouvain.be, roussin.lontio@gmail.com (R.o.s. Lontio Fomekong).

http://dx.doi.org/10.1016/j.jssc.2016.06.012
0022-4596/

precipitation followed by thermal decomposition [18]. In particular, the latter is simple, low cost, well controlled and readily yields high purity products. With this method, it is possible to add one or more surfactants to influence the final particle size. In fact, it has been demonstrated that a surfactant has a great influence on the particle size of the material [19].

Oleylamine (OAm) is a long-chain primary alkylamine surfactant which, just like octadecylamine (ODA) or hexadecylamine (HDA), can act as an electron donor at high temperatures. Interestingly, commercial OAm has a much lower cost than commonly used pure alkylamines, though some concerns regarding purity and reproducibility have also been raised [19]. Moreover, the fact that OAm is liquid at room temperature, may facilitate the washing procedures that follow the chemical synthesis of nanoparticles. However, care should be taken in handling OAm since, as indicated in the material safety data sheet, it can be corrosive to the skin [19].

While a search in the literature shows that the thermal decomposition of many metal malonates [20,21] and in particular nickel malonate [22,23], have been investigated, the latter study addressed the synthesis of NiO nanoparticles from such a precursor and the influence of the surfactants on this synthesis seems to be scarce [24]. We, thus, provide in this article, ample evidence that oleylamine is an effective surfactant for the size reduction of the of NiO nanoparticles obtained via the pyrolysis of nickel malonate pre-synthesized by precipitation.

2. Experimental section

2.1. NiO synthesis

Hydrated nickel chloride ($NiCl_2 \cdot H_2O$), hydrated lithium hydroxide ($LiOH \cdot H_2O$), malonic acid ($HOOCCH_2COOH$) and the surfactant, oleylamine ($CH_3(CH_2)_7CH{=}CH(CH_2)_8NH_2$), all obtained from Aldrich, ethanol and acetone obtained from MERK were used without further purification.

NiO nanoparticles were obtained via two experimental steps: the synthesis of the precursor and its subsequent decomposition. Two syntheses were carried out for the precursor. In the first synthesis (without any surfactant), the precursor, nickel malonate ($NiCH_2C_2O_40 \cdot 2H_2O$), code-named NiM, was prepared according to the procedure described in the literature [25] and calcined in a ceramic combustion boat holder at 500 °C in a muffle oven at a heating rate of 10 °C/min for 1 h under air flow. In the second synthesis (with the surfactant), 1.2 g of the previously synthesized nickel malonate were placed in a round bottom flask, 10 mL of oleylamine added and the mixture heated, with continuous stirring, in an oil bath for 1 h at 140 °C. The resulting light green solution was cooled to room temperature and an excess of ethanol added. The green precipitate obtained after filtration was washed several times with ethanol and dried at 100 °C for 4 h (Scheme 1). The precursor, modified by the surfactant and code-named NiMO, was calcined in a ceramic combustion boat holder at 500 °C in a muffle oven at a heating rate 10 °C/min for 1 h under air flow.

2.2. Characterization methods

The two synthetized precursors were characterized by FTIR and TGA, and the decomposition products by XRD, SEM, TEM and BET.

The functional groups of the malonate ligand and the oleylamine were elucidated using Fourier Transform Infra-Red (FTIR) spectroscopy on the QuickLock Single Reflection Horizontal ATR Accessory from Bruker. The Thermal behavior of the precursor was studied by Thermogravimetry Analysis (TGA) on a METTLER TOLEDO Thermal Analyzer in air and in nitrogen at a flow rate of 100 mL min^{-1}, in the temperature range 25–900 °C and at a heating rate of 10 °C min^{-1}. The presence of oleylamine in the NiMO precursor was confirmed using Time of Flight Secondary Ions Mass Spectrometry (ToF-SIMS) on an IONTOF V spectrometer (IONTOF GmbH, Munster, Germany). The samples were initially bombarded with Bi_5^+ ions (30 keV, 45°) and the resulting secondary ions accelerated at 2 kV before entering the analyzer and post-accelerated at 10 kV before detection. The surface area of analysis was $200 \times 200\ \mu m^2$, the data acquisition time was 2 min and the primary ion dose was 4.12×10^7 ions cm^{-2}. The Powder X-ray Diffraction (PXRD) data for the decomposition products were collected at room temperature with a D5000 Siemens Kristalloflex $\theta - 2\theta$ Powder Diffractometer. This diffractometer had a Bragg-Brentano geometry and was equipped with a graphite-monochromated Cu-Kα ($\lambda = 1.54056$ Å) radiation, a standard scintillation counter detector and an automatic sample changer which could accommodate 30 samples. For the experiment, the decomposition products were spread out on a flat silicon plate in such a manner as to avoid preferred orientations. The patterns were recorded in the range of 5–90° with a scan step of 0.02° (2θ) and a 2 s $step^{-1}$ acquisition interval. These patterns were compared to the NiO pattern of the ICCD using HighScore Plus Software for phase identification. The recorded patterns were also indexed and the unit cell refined by using the FullProf-suite program [26]. The morphology of the decomposition products was determined by Scanning Electron Microscopy (SEM) using a high resolution FEG JEOL7600F with an accelerating voltage of 15 kV. The images were obtained with the semi-in-lens secondary electron detector. The particle sizes were also estimated by SEM. The morphologies of the samples were confirmed by transition electron microscopy (TEM, Leo922 Model from Zeiss) with an accelerating voltage of 120 kV. TEM samples were prepared by dropping a sonicated water dispersion suspension of the powder samples on a carbon-coated copper grid. Textural analyses were carried out on Micromeritics Tristar 3000 equipment using N_2 adsorption/desorption at 77.150 K. Samples were degassed under

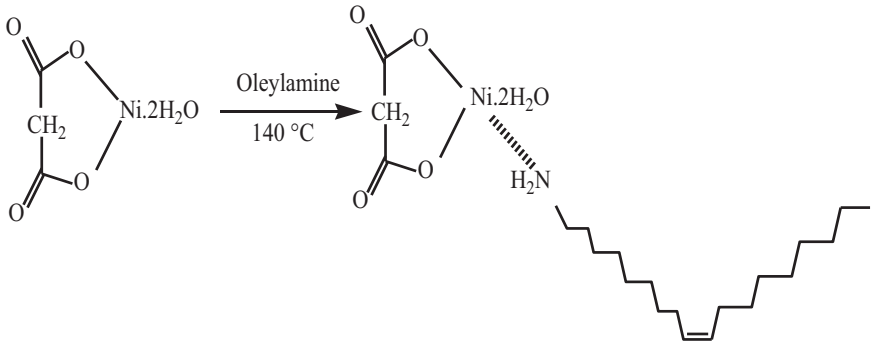

Scheme 1. Illustration of the reaction between nickel malonate and oleylamine.

vacuum at 150 °C for a period of at least 12 h prior to surface area measurement. The specific surface area was calculated using the Brunauer–Emmet–Teller (BET) equation whereas the pore size distributions were derived from the desorption branches using the Barrett–Joyner–Halenda (BJH) model.

3. Results and discussion

FTIR spectrometry was performed in order to verify that the ligand (malonate) and the surfactant (oleylamine) are effectively present in the precursor. The two spectra (Fig. 1) clearly show the absorption bands corresponding to the malonate ligand, as corroborated by the literature [25]. However, there are two major differences between the two precursors, NiM and NiMO. The first difference is that, for the NiMO precursor, one additional absorption band is observed at 1053 cm^{-1}, which can be assigned to the bending vibration of the C-N bond indicating the presence of the oleylamine molecule. The second difference is that the intensities of all the absorption bands are higher for the NiMO precursor than those of NiM. The increase in the observed absorption intensities can be explained on the basis of the similarity between the characteristic functional groups of oleylamine and those of nickel malonate. In other words, the presence of oleylamine in the nickel malonate precursor will tend to increase the intensities of the existing absorption bands. The absorption bands observed at 3453 cm^{-1} and 3185 cm^{-1} can be ascribed, respectively, to lattice water present in the nickel malonate and the symmetric and asymmetric stretching vibrations of -NH_2 present in oleylamine. The bands at 2920 and 2852 cm^{-1} correspond, respectively, to the asymmetric and symmetric stretching vibrations of the C–H bonds which are present in both the malonate ligand and oleylamine. The bands at around 1660 cm^{-1} and 1560 cm^{-1} can be assigned to the OCO asymmetric stretching vibrations of the carboxylate group present in the nickel malonate and to the bending vibrations of –C═C and -NH_2 bonds, respectively, present in oleylamine. The closeness of these values to those in the literature [19,25] confirms that the malonate ligand and the oleylamine are effectively present in the NiMO precursor. This implies that the nickel malonate was successfully modified by oleylamine via our synthetic route.

To further confirm the presence of oleylamine in the NiMO precursor and to study its thermal behavior, themogravimetric analyses (TGA) were carried out in air and nitrogen and the results are shown in Fig. 2. The TGA of NiM in air has already been

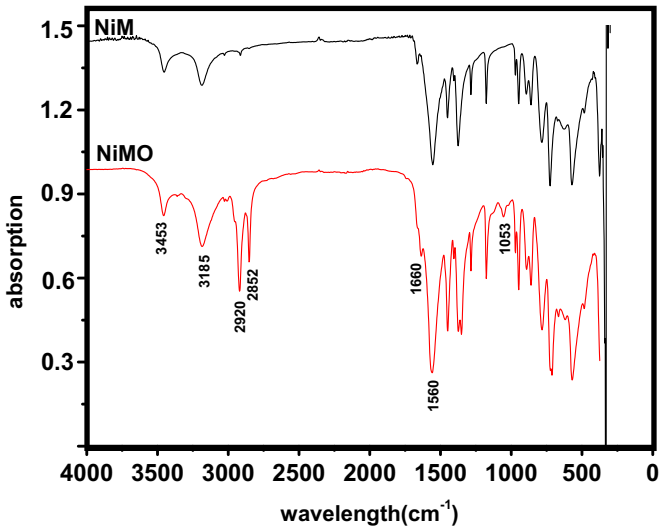

Fig. 1. FTIR spectra of NiM and NiMO.

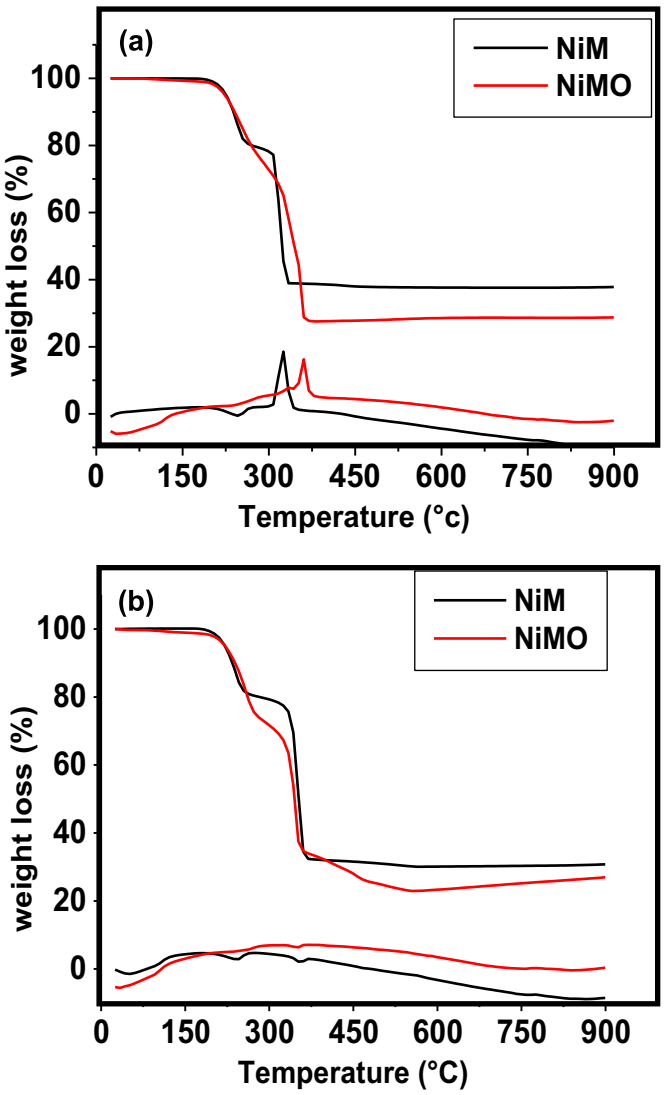

Fig. 2. Thermogravimetry of NiM and NiMO in air (a) and in nitrogen (b).

published in our previous paper [25]. Hence, we shall focus here on the NiMO precursor. Two main weight losses are observed between 25 °C and 900 °C for both precursors and the weight loss is more important for NiMO than NiM, which indicates the presence of a larger quantity of organic compounds (malonate and oleylamine) in NiMO. The first weight loss is attributed to dehydration or loss of water molecules [25]. In air (Fig. 2(a)), the inorganic residue after thermal decomposition constitutes 37.60%, corresponding to NiO in the case of the NiM (37.94% expected) and 28.66% in the case of the NiMO (28.34% expected, assuming one oleylamine for four nickel malonate molecules). The TG curves show that the precursor decomposes at 343 °C for NiM and 360 °C for NiMO which indicates that the presence of oleylamine does not affect much the decomposition temperature of the precursor. In nitrogen (Fig. 2(b)), the inorganic residue after thermal decomposition constitute 30.06% (29.85% expected), corresponding to metallic nickel for NiM and 22.93% (22.27% expected, again assuming one oleylamine for four nickel malonate molecules) in the case of the NiMO. The results obtained in nitrogen corroborate those measured in air.

The presence of Oleylamine in the NiMO precursor was confirmed by ToF-SIMS. For this purpose, the NiM and NiMO precursors were analyzed and the positive and negative mass spectra are shown in Fig. 3. In the negative spectra (Fig. 3(a)), two

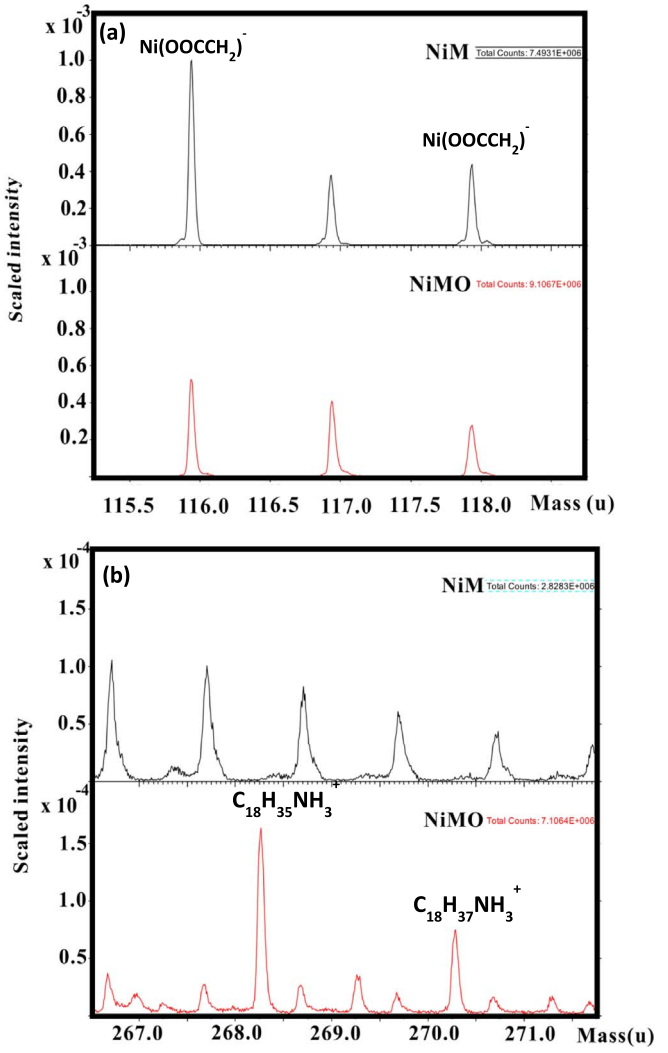

Fig. 3. Partial negative (a) and positive (b) ToF-SIMS spectra of NiM and NiMO precursors.

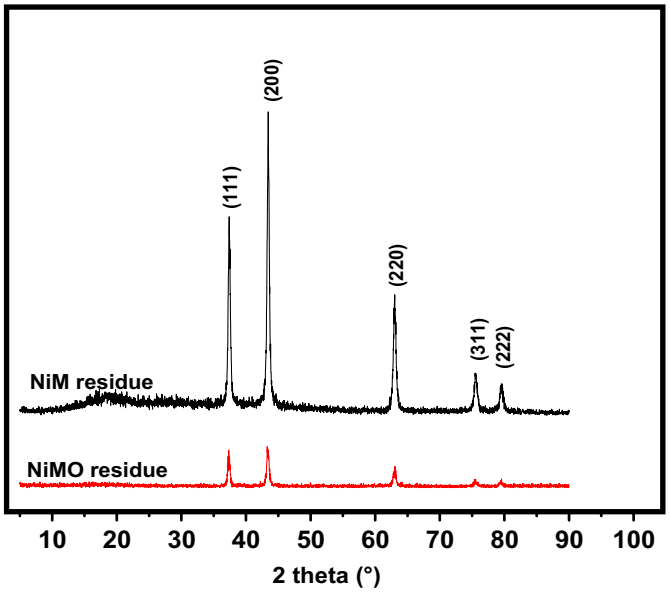

Fig. 4. Powder XRD of NiM and NiMO decomposition products.

significant peaks are present at *m/z* 116 and 118 in both the NiM and the NiMO precursors, corresponding to $Ni(OOCCH_2)^-$ with the expected isotopic ratio. These peaks confirm the presence of nickel malonate in the two samples. Fig. 3(b) shows the region of the positive mass spectra corresponding to the mass of the oleylamine molecular ion moiety. The mass spectrum of the NiMO precursor exhibits intense ion peaks attributable to $C_{18}H_{35}NH_3^+$ (*m/z* 268) and $C_{18}H_{37}NH_3^+$ (*m/z* 270) which are absent in NiM. These additional peaks confirm the presence of oleylamine ($C_{18}H_{35}NH_2$) in NiMO, demonstrating the effective modification of the nickel malonate by the surfactant. The other peaks observed in the mass spectra of the two precursors are associated with the nickel malonate ion cluster.

These results suggest a simple Van der Waals (weak) interaction (see Scheme 1) between the nitrogen of the amine group of the oleylamine and the nickel ion. The evidence for this comes from the absence of the absorption band of Ni–N bond in the FTIR spectrum and the fact that there is no peak associated with the Ni-oleylamine fragment in the ToF-SIMS spectrum. This observation is in accordance with the literature [19].

The XRD patterns of the two samples are shown in Fig. 4. They indicate that the decomposition products for the NiM and NiMO precursors are the same. These products were identified as the cubic NiO (*Fm*-3*m*) phase (*ICDD ref N°: 04–007-8202*) [27]. However, for the precursor containing oleylamine (NiMO), the decomposition product shows peaks with smaller intensities and slightly larger integral widths compared to the sample obtained with the NiM precursor containing only nickel and the malonate ligand. These phenomena could be attributed, respectively, to the decrease of the crystallinity and the reduction of the particle size of the decomposition products in the presence of the surfactant during the pyrolysis process.

SEM analysis was also carried out to ascertain the size and morphology of the particles after the decomposition process and the results are presented in Fig. 5. As the micrographs show, the polycrystalline nature, with well-defined spherical nanoparticles, of the decomposition products of the two precursors, NiM and NiMO (Fig. 5(a) and (b), respectively) is obvious. This result means that the surfactant (oleylamine) does not affect the particle morphology but obviously affects the particle sizes. The particle sizes were averaged over 50 particles in each case and the corresponding histograms reveal that most of the particles are in the range of 70–80 nm for the NiO obtained from the NiM precursor (Fig. 5(c)) and, in the range of 25–35 nm for those obtained from NiMO (Fig. 5(d)). NiO nanoparticles obtained by the thermal decomposition of the NiMO precursor are smaller in size (mean size 33 ± 6 nm) than those obtained for NiM (mean size 72 ± 15 nm), corresponding to a 54% particle size reduction due to the oleylamine surfactant. This result is corroborated by that from TEM (Fig. 6) which shows that in the presence of oleylamine, there is almost no agglomeration of particles thus resulting in the uniformity of particle sizes (Fig. 6(b)) which is not the case in the absence where we can observe a large agglomerate (Fig. 6(a)). This phenomenon may be explained on the basis of the fact that the presence of cumbersome molecules like the oleylamine surfactant in the precursor reduces the interaction (through steric hindrance) between adjacent nickel malonate molecules. This, therefore, limits considerably the possibility of agglomeration of the nanoparticles during the thermal decomposition process. This observation is in agreement with that reported in the literature [24].

The nitrogen adsorption–desorption isotherm curves of the NiO synthesized by thermal decomposition of NiM and NiMO are presented on Fig. 6. The adsorption isotherm of the two samples is of type III and they differ only by the amount of adsorbed N_2, which follows the respective specific surface areas of the samples as presented in Table 1. The NiO synthesized by the thermal decomposition of NiMO has a larger specific surface area and adsorbs

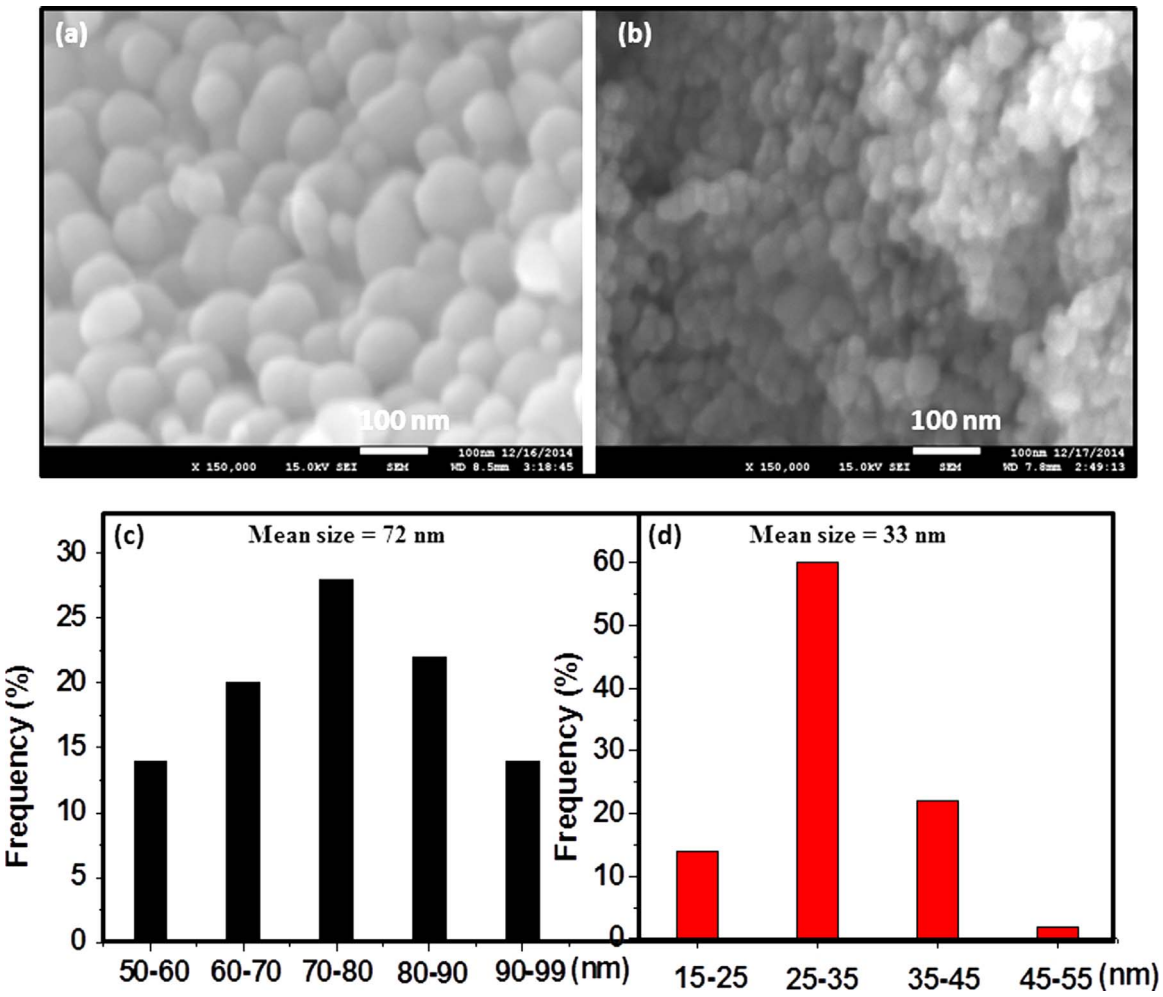

Fig. 5. SEM images and the particle size distributions of decomposition products of NiM (a), (c) and NiMO (b), (d).

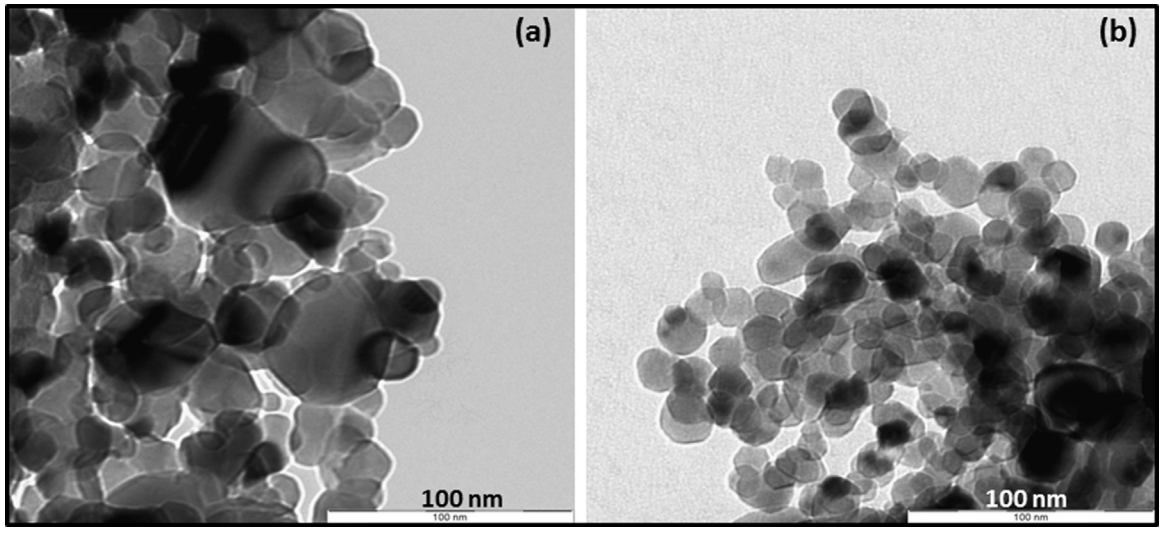

Fig. 6. TEM images of decomposition products of NiM (a) and NiMO (b).

Table 1
Specific surface area values and the pore volumes of the synthesized NiO.

Samples	S_{BET} (m^2/g)	Pore volume (cm^3/g)
NiO from NiM	4	0.018
NiO from NiMO	19	0.060

more nitrogen than the one obtained from NiM. As for the NiO obtained from NiM, the desorption and adsorption isotherms perfectly overlap indicating that the NiO is non-porous. On the other hand, the NiO obtained from NiMO shows a little capillary decondensation thus indicating the presence of small mesopores. The difference in the porosity structures of the two NiO is

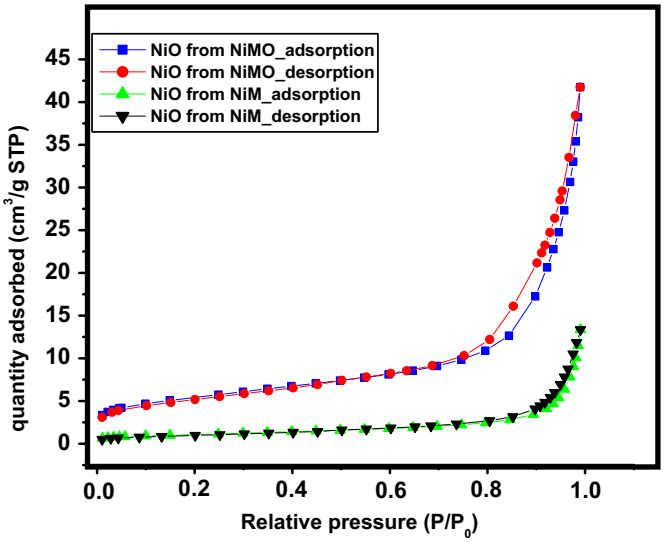

Fig. 7. Nitrogen physisorption isotherms of the NiO obtained from NiM and NiMO.

confirmed by the measurement of the pore volume. The specific surface area values and the pore volumes obtained are summarized in Table 1. As these results indicate, the surface area of the NiO and the pore volume increase significantly in the presence of surfactant (4.75 and 3 times, respectively, larger for NiMO than for NiM). These results are in concordance with those of SEM and XRD. In addition, it is a well-established fact that for a spherical particle, a reduction in size induces an increase in the specific surface area [28].Fig. 7.

4. Conclusion

The reduction in the nanoparticle sizes of NiO obtained via the pyrolysis of nickel malonate pre-synthesized by precipitation has been successfully achieved by a simple modification of the precursor using oleylamine as surfactant. The new precursor obtained (nickel malonate-oleylamine) was characterized by FTIR and TGA and ToF-SIMS analyses. The reduction in the NiO nanoparticle sizes, as demonstrated by SEM and TEM, was found to be in agreement with the XRD and BET results. The nanoparticle size reduction was attributed to the presence of oleylamine in the modified precursor which limits agglomeration during the thermal decomposition of the precursor. The particle size reduction observed increases significantly the specific surface area of NiO as revealed by BET. The synthesis method employed is inexpensive and reproducible with a potential for upscaling and can be readily extended to the synthesis of other metal oxide nanoparticles especially where size is an important factor.

Acknowledgment

The authors sincerely thank “Université Catholique de Louvain (UCL) (SPER/DST/525–1122601)” for funding Mr. Roussin LONTIO FOMEKONG in the scholarship program “Cooperation au développement” in Belgium, where the main part of the work reported in this paper was carried out. The authors also thank Claude POLEUNIS and Eric GAIGNEAUX and Pascale LIPNIK for their help in the physicochemical analysis of the products.

References

[1] E. Roduner, Chem. Soc. Rev. 35 (2006) 583–592.
[2] A.K. Alves, F.A. Berutti, F.A.L. Sánchez, Nanostructured Materials for Engineering Applications, Springer Berlin, Heidelberg Berlin, 2011.
[3] R. Bogue, Sens. Rev. 34 (2014) 1–8.
[4] H. Kamal, E.K. Elmaghraby, S.A. Ali, K. Abdel-Hady, J. Cryst. Growth 262 (2004) 424–434.
[5] J.-M. Choi, S. Im, Appl. Surf. Sci. 244 (2005) 435–438.
[6] J.F.K. Cooper, A. Ionescu, R.M. Langford, K.R.A. Ziebeck, C.H.W. Barnes, R. Gruar, C. Tighe, J.A. Darr, N.T.K. Thanh, B. Ouladdiaf, J. Appl. Phys. 114 (2013) 083906 (1)-083906(7).
[7] L. Yuan, Z.P. Guo, K. Konstantinov, P. Munroe, H.K. Liu, Solid-State Lett. 9 (2006) A524–A528.
[8] J. Bandara, H. Weerasinghe, Sol. Energy Mater. Sol. Cells 85 (2005) 385–390.
[9] C.G. Granqvist, G.A. Niklasson, A. Azens, Appl. Phys. A – Mater. Sci. Proc. 89 (2007) 29–35.
[10] J.G. Cheng, L.P. Deng, B.R. Zhang, P. Shi, G.Y. Meng, Rare Met. 26 (2007) 110–117.
[11] K.B.M. Ghosh, A. Sundaresan, C.N.R. Rao, J. Mater. Chem. 16 (2006) 106–111.
[12] A.M. Soleimanpour, A.H. Jayatissa, G. Sumanasekera, Appl. Surf. Sci. 276 (2013) 291–297.
[13] X. Song, L. Gao, S. Mathur, J. Phys. Chem. C 115 (2011) 21730–21735.
[14] E.R. Beach, K. Shqau, S.E. Brown, S.J. Rozeveld, P.A. Morris, Mater. Chem. Phys. 115 (2009) 371–377.
[15] M. Alagiri, S. Ponnusamy, C. Muthamizhchelvan, J. Mater. Sci. Mater. Electron. 23 (2012) 728–732.
[16] X. Song, L. Gao, J. Am. Ceram. Soc. 91 (2008) 3465–3468.
[17] K.G. Chandrappa, T.V. Venkatesha, K.O. Nayana, M.K. Punithkumar, Mater. Corros. 63 (2012) 445–455.
[18] X. Wang, J.M. Song, L.S. Gao, J.Y. Jin, H.G. Zheng, Z.D. Zhang, Nanotechnology 16 (2005) 37–39.
[19] S. Mourdikoudis, L.M. Liz-Marzán, Chem. Mater. 25 (2013) 1465–1476.
[20] B.S. Randhawa, K. Gandotra, J. Therm. Anal. Calorim. 28 (2006) 417–424.
[21] K. Muraishi, K. Nagase, N. Tanaka, Thermochim. Acta 23 (1978) 125–133.
[22] V. Mathew, K.C. Mathai, C.K. Mahadeven, K.E. Abraham, Physica B 406 (2011) 426–429.
[23] K.A. Jones, R.J. Acheson, B.R. Wheeler, A.K. Galwey, Trans. Faraday Soc. 64 (1968) 1887–1897.
[24] Y. Bahari Molla Mahaleh, S.K. Sadrnezhaad, D. Hosseini, J. Nanomater. 2008 (2008) 1–4.
[25] R. Lontio Fomekong, P. Kenfack Tsobnang, D. Magnin, S. Hermans, A. Delcorte, J. Lambi Ngolui, J. Solid State Chem. 230 (2015) 381–389.
[26] T. Roisnel, J. Rodríguez-Carvajal, WinPLOTR: a windows tool for powder diffraction pattern analysis, Mater. Sci. Forum (2001).
[27] J.H. Binks, J.A. Duffy, J. Solid State Chem. 87 (1990) 195–201.
[28] S. Majumdar, Cerem. Int. 41 (2015) 14350–14358.